AIAA 80-0157R

Application of the Adaptive Wall Concept in Three Dimensions

R. L. Parker Jr.* and W. L. Sickles†
ARO, Inc., Arnold Air Force Station, Tenn.

The adaptive wall concept requires that to obtain unconfined flow conditions in a wind tunnel in the presence of any model it is necessary and sufficient to match independent measured flow variables on a surface near the tunnel boundary with flow variables which satisfy the unconfined, undisturbed boundary condition at infinity. The technique was employed at a limited number of test conditions to adjust individually the variable porosity walls of the AEDC Aerodynamic Wind Tunnel (4T) in order to minimize wall interference effects on a generalized transonic model configuration. Data improvement was demonstrated for each set of conditions. A procedural description and results of the experiment are presented.

Nomenclature

C_D = drag coefficient
C_L = lift coefficient
C_m = pitching moment coefficient
C_P = pressure coefficient
CTS = captive trajectory system
h = tunnel width
k = relaxation factor
M_∞ = Mach number
P = pressure
S = control surface
s = model wing span
v = perturbation velocity normal to top and bottom walls
w = perturbation velocity normal to side walls
x = longitudinal dimension
y = lateral dimension, see Fig. 3
z = vertical dimension, see Fig. 3
α = angle of attack
τ = wall porosity, %
ϕ = perturbation velocity potential (nondimensionalized)

Subscripts

e = external region
T = measured in tunnel
x = streamwise coordinate
y = horizontal normal coordinate
z = vertical normal coordinate

Superscript

n = number of iterations

Introduction

THE adaptive wall development program at Arnold Engineering Development Center (AEDC) has included two-dimensional, transonic experiments in the Aerodynamic Wind Tunnel (1T).[1] It was observed in these experiments that there were general features of the distribution of flow variables at the control surface which were critical for reducing or eliminating interference at the model location. Namely, it was important that the flow approaching the model be properly adjusted to the freestream value and that the minimum pressure at the control surface be in agreement with that computed for unconfined flow (Fig. 1). One of the configurations investigated in these experiments was simply a uniformly variable porosity wall similar to that of the AEDC Aerodynamic Wind Tunnel (4T) with the standard transonic wind-tunnel single-plenum arrangement. It was found that porosity adjustment, in conjunction with plenum pressure control, was effective for adjusting the pressure on the control surface in a global sense. When the value of the minimum pressure was correctly adjusted, the variable porosity walls also yielded a reasonable approximation of the remainder of the required control surface pressure distribution.

A conclusion from these experiments was that adaptive wall techniques could be employed in a wind tunnel with some form of wall control, such as variable porosity, to provide a viable procedure for adjusting the walls to eliminate or minimize the interference on a model. Preliminary experiments were conducted in Tunnel 4T with a simplified wing/tail/body model to evaluate the effectiveness of the globally variable porosity capability for adaptive wall control and to identify problem areas for three-dimensional adaptive wall development. Iterative wall adjustments were carried out online for a limited number of test conditions. Significant improvement in the model data was demonstrated by comparing these data to wall interference-free reference data obtained with the model in the AEDC Aerodynamic Wind Tunnel (16T).

Adaptive Wall Method

According to the concept of the adaptive wall wind tunnel, as stated in Refs. 2-4, to obtain unconfined flow conditions in a tunnel with any model it is necessary (and sufficient) to match the measured flow variables on a selected control surface S (Fig. 2) with the flow variables that satisfy the unconfined boundary condition. Specifically, one needs to measure the distributions of two independent flow variables, such as the normal component of velocity and the pressure on the control surface located inside the tunnel but away from the model. One of the measured distributions is used as the boundary condition to determine the flowfield exterior to S in the presence of unconfined, undistributed flow at infinity. Since the two measured distributions constitute redundant boundary data for the exterior boundary value problem, a comparison of the exterior region calculated values with the measured values of the same quantities determines whether or not unconfined-flow conditions exist in the tunnel. In general, wall boundary adjustments must be made in an iterative manner until unconfined conditions do exist.

Three-Dimensional Exterior Computational Method

The three-dimensional flowfield exterior to and including the control surface S is assumed outside the region of large

Presented as Paper 80-0157 at the AIAA 18th Aerospace Sciences Meeting, Pasadena, Calif., Jan. 14-16, 1980; submitted Jan. 16, 1980; revision received May 27, 1980.

*Project Engineer, 4T Projects Branch, Propulsion Wind Tunnel Facility, AEDC Division. Member AIAA.

†Research Engineer, 4T Projects Branch, Propulsion Wind Tunnel Facility, AEDC Division.

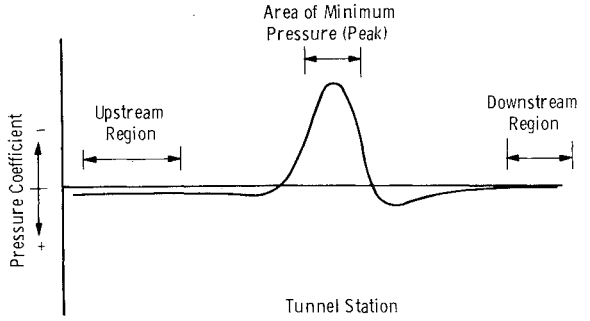

Fig. 1 Critical regions of control surface pressure distributions as identified in two-dimensional experiments.

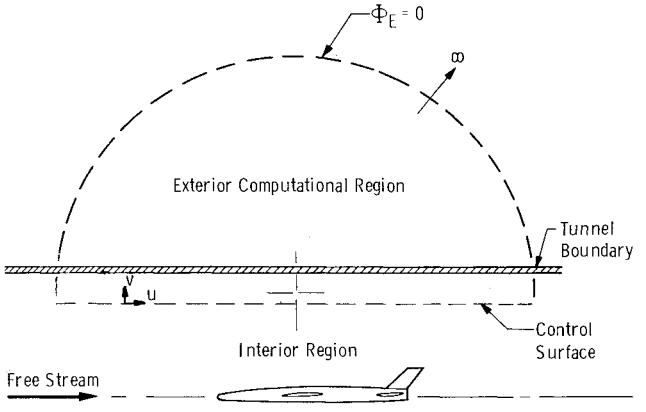

Fig. 2 Adaptive wall concept.

disturbances and complicated viscous flow existing in the vicinity of the model. Also, it is assumed that S is outside the tunnel wall boundary-layer region. Under these assumptions, the exterior flowfield is adequately represented by the transonic small-disturbance equation of the form

$$\left[\left(1-M_\infty^2\right)\phi_x-\frac{\gamma+1}{2}M_\infty^2\phi_x^2\right]_x+[\phi_y]_y+[\phi_z]_z=0 \qquad (1)$$

with the boundary conditions shown in Fig. 3. The distribution of normal velocity measured in the tunnel is specified as the boundary condition at S. An unconfined-flow boundary condition is assumed and specified at a distance of four tunnel heights, assumed to be infinity, from the control surface for the test in Tunnel 4T. A symmetry boundary condition is used at $y=0$. The boundary conditions at the upstream and downstream planes are selected as $C_P=0$ where the upstream plane is located 40 in. upstream of the model nose and the downstream plane is located 26 in. downstream of the model tail. The survey locations at the control surface are presented in Fig. 4. Because of the limited travel of the measuring apparatus at the control surface, the values of the normal velocity component v_T are extrapolated upstream to the test section entrance, where v_T is assumed to be zero, and downstream to the test section exit, where v_T is assumed to be a constant equivalent to the downwash angle of the farthest downstream measurement. The boundary condition w_T on the lateral surface is assumed to be zero. This assumption was made for reasons discussed in the Results section and, as will be demonstrated, was an acceptable assumption for this experimental configuration.

A program has been developed to solve numerically this boundary value problem using the Murman finite-difference method in Ref. 5 as modified by Bailey and Ballhaus[6] for three-dimensional transonic computations. The finite-difference equations are developed using central-difference operators in the subsonic region, upwind differences in the

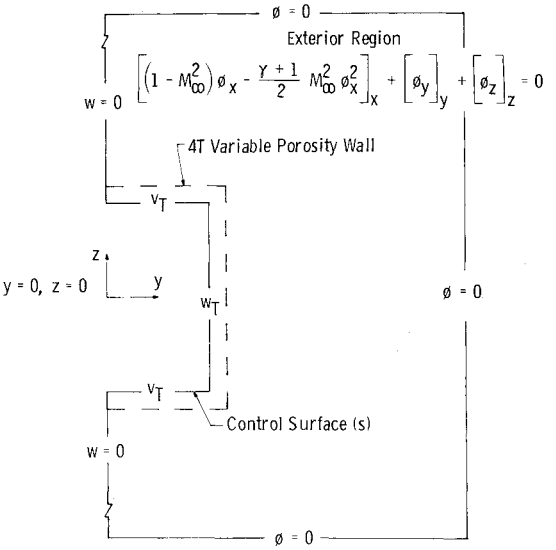

Fig. 3 Three-dimensional boundary value problem for exterior region.

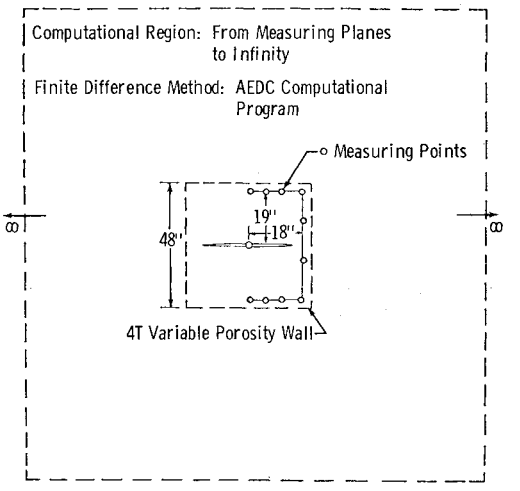

Fig. 4 Adaptive wall configuration for Tunnel 4T.

supersonic region, and a special shock operator to give the correct jump conditions. These difference equations are solved using the iterative technique of successive line over-relaxation (SLOR). The program iterates until the residuals of the velocity potentials are within a tolerance of 1×10^{-4}.

The program requires approximately 190K bytes of storage for an x-y-z mesh of $40\times20\times30$. A typical run takes 200 iterations and executes in 7 min of CPU time on the IBM 370 computer. On the first iteration the program calculates the exterior region starting from a zero potential field and stores the result in a restart file. Successive iterations use the restart file from the previous iterations as the initial potential field. This restart capability reduces the number of numerical iterations and computer time to achieve convergence by one-half.

Apparatus

Tunnel 16T

The Propulsion Wind Tunnel (16T) is a closed-loop, continuous-flow, variable-density tunnel in which the Mach number can be varied 0.2-1.6 and the stagnation pressure 120-4000 psf. The test section is 16 ft square and 40 ft long with 60 deg inclined-hole perforated walls of 6% porosity. A more complete description can be found in Ref. 7.

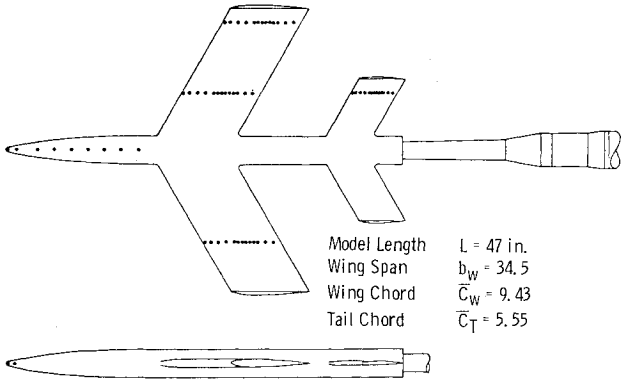

Fig. 5 Three-dimensional wall interference model.

Tunnel 4T

The Aerodynamic Wind Tunnel (4T) is a closed-loop, continuous-flow, variable density tunnel in which the Mach number can be varied 0.1-1.3 and also can be set at 1.6 and 2.0 by placing nozzle inserts over the permanent sonic nozzle. The test section is 4 ft square and 12.5 ft long with perforated, individually variable porosity (0.5-10% open) walls. It is enclosed in a plenum chamber from which the air can be evacuated, allowing part of the tunnel airflow to be removed through the perforated walls of the test section. A more complete description can be found in Ref. 7.

Flowfield Probe

The probe employed for the control surface variable measurements is a 40 deg included angle, conical head probe with four static pressure orifices equally spaced around the conical surface and a total pressure orifice at the cone apex. The probe was supported by a straight cylindrical extension attached to the Tunnel 4T captive trajectory system (CTS). An offset was provided at the attachment point to the CTS to allow the probe to be placed within 4 in. of the top and south test section walls by the normal CTS movement.

Model

The test model was specially designed for wall interference studies and consisted of a swept wing/tail and body combination. The model size was chosen to produce measurable wall interference in Tunnel 4T. The solid blockage ratio in Tunnel 4T is 1.33% and the ratio of wing span to tunnel width is 0.72. The lifting sections have NACA-0012 profiles normal to the leading edge, and the sweep angle is 30 deg. The model has both lateral and vertical symmetry. There are chordwise rays of pressure orifices at the 40 and 90% span locations of the right wing and at the 65% span location of the left wing. There is a chordwise ray of orifices at the 78% span location on the right tail. Each chordwise ray of orifices consists of 13 orifices on the upper surface and 4 orifices on the lower surface. There is a ray of orifices on the upper forebody surface, and the model nose is designed as a five-orifice, hemispherical head flow angle meter. The model contains two 48-port Scanivalves® internally with ±15 psi strain-gage-type transducers and a six-component force balance. The model geometry is shown in Fig. 5.

Test Description

Interference-Free Data

A test was conducted in the Aerodynamic Wind Tunnel (16T) to obtain wall interference-free data for the model. The model solid blockage ratio in Tunnel 16T is 0.083%. Model force and pressure data were obtained. The model was sting-mounted from a strut support, which was mounted in the floor of the test section.

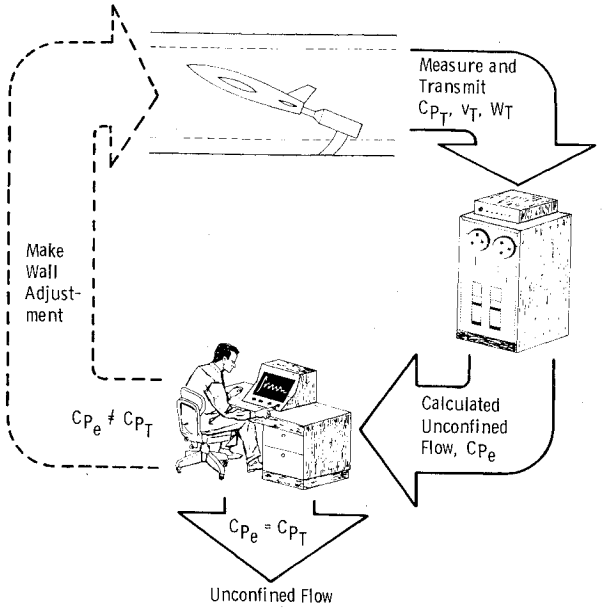

Fig. 6 Experimental iterative procedure.

Implementation of the Adaptive Wall Technique in Tunnel 4T

The iterative procedure for adjusting the 4T walls by the adaptive technique is presented in the block diagram in Fig. 6. First a flowfield is established in the tunnel at the desired conditions. The model attitude is defined as the angle relative to the plane of the top and bottom walls. The distribution of the flow angle and static pressure are measured at the control surface, which was selected to be a surface 5 in. from the interior surface of the test section walls (see Figs. 3 and 4). Linear relations are employed to convert the flow angle and pressure coefficient to the perturbation velocities normal and parallel to the freestream, respectively. The number and location of the measurements must be adequate to permit interpolation of the variables over the entire control surface.

The measured control surface data are reduced to engineering units by the tunnel computer and transmitted to an IBM 370/165 disk file. The exterior computational region is then evaluated by inputting the measured data results to the three-dimensional adaptive wall program. The program converts the measured data to the perturbation velocities, u and v, performs the exterior flow calculation by specifying the normal velocity v as the boundary condition on S, and stores the results and the corresponding data measured at the surface in a graphics file. The above procedure is controlled from the interactive graphics terminal in the Tunnel 4T control room.

Comparison of the distribution of pressure on the control surface for unconfined flow as calculated by the exterior program C_{P_e} and that measured in the tunnel C_{P_T} are made at the graphics terminal. The measured data were actually displayed as a line spline fitted to the results of a weighted, smoothing routine. If the distributions do not agree, the wall porosities are adjusted. The procedure continues until the best agreement between C_{P_e} and C_{P_T} is obtained.

Wall control in Tunnel 4T is limited to global porosity adjustment without a longitudinal or lateral variation capability. This necessitates matching the desired control surface distribution in a global sense rather than in a local sense. As discussed in Ref. 1, the dominant criterion for this adjustment is the value of the peak, or minimum pressure, on the control surface.

To accelerate convergence, a relaxation factor k is introduced in the iterative procedure as

$$C_p{}^{(n+1)} = kC_{P_e}{}^{(n)} + (1-k)C_{P_T}{}^{(n)} \text{ at } S \qquad (2)$$

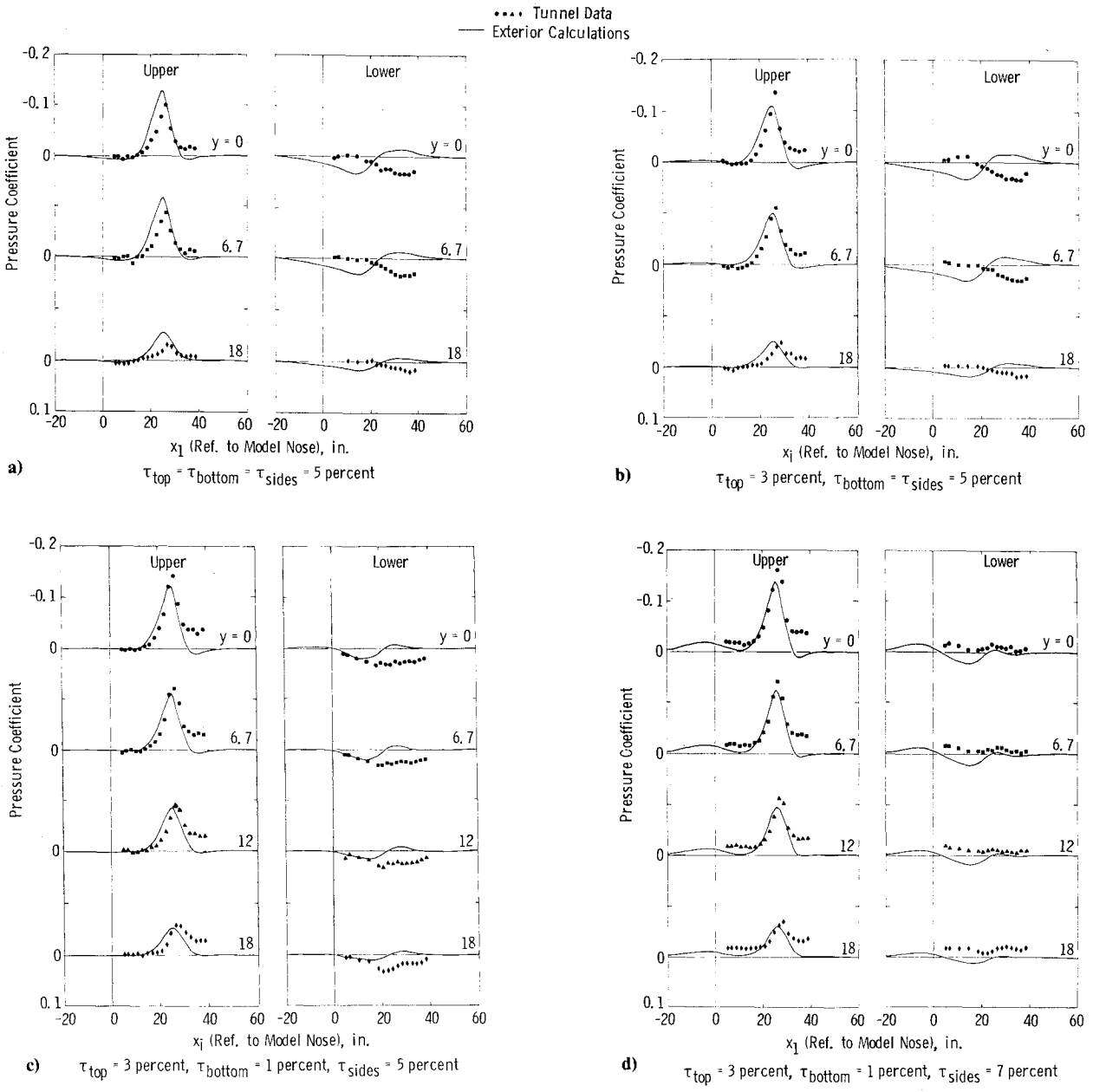

Fig. 7 Control surface presure distribution, $M_\infty = 0.9$ and $\alpha = 4$ deg.

The wall adjustment procedure is performed according to Eq. (2) with $k = 0.5$. In the present experiment, wall porosity adjustments were expedited by changing, in order, the top wall, bottom wall, and then the side walls. This procedure worked well; however, if the procedure were automated the adjustments could be made simultaneously.

Test Procedure (Tunnel 4T)

Operation of the CTS and main pitch sector was controlled by the digital computer that automatically set the model angle of attack, positioned the probe at a reference location, and controlled the probe movement through commands to the CTS to preselected positions. At each position, the wind-tunnel operating conditions and the probe pressures were measured and recorded. The probe pressures were then reduced to pressure coefficients and flow angles and tabulated in summary form after each survey was completed. The control surface data were obtained as the probe was moved downstream at a given y and z position. When force and pressure data for the model were acquired at the selected model attitudes and tunnel conditions, the CTS was moved to its most aft and up position.

It should be noted that the Tunnel 4T CTS capabilities placed some constraints on this experimental program. To prevent physical interference between the pitch sector and the CTS, the model attitude was limited to a 4 deg angle of attack. The CTS travel is also limited to the upper half of the test section. Therefore, the lower control surface information was obtained by placing the model at an equal, negative incidence; adjusting the wall porosity accordingly; obtaining measurements at the upper tunnel control surface; and converting them as if for the lower control surface.

The CTS longitudinal travel also limited the probe position to an area extending approximately 5-40 in. aft of the model nose location. As discussed previously, the values of the measured flow variables were interpolated from the limits of the probe travel to the test section extremities.

Results

To obtain a large model disturbance, an angle of attack of 4 deg, the maximum pitch angle obtainable with the CTS installed, was selected at Mach numbers 0.7, 0.9, and 0.95. All data presented were obtained at a tunnel total pressure of 1500 psf. At Mach number 0.7, the flow over the model is

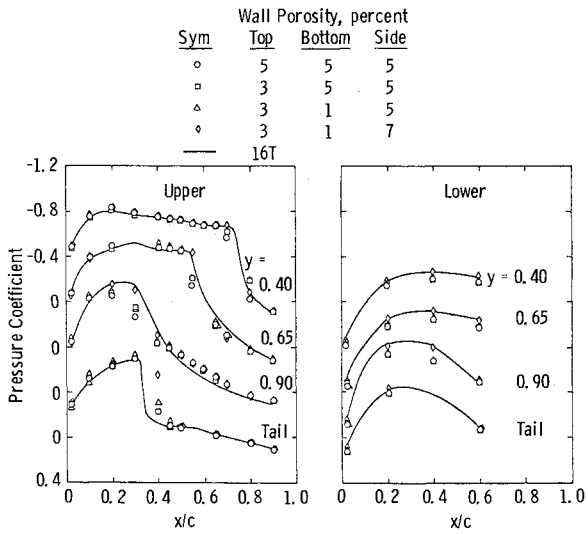

Fig. 8 Model wing and tail pressure distribution, $M_\infty = 0.9$ and $\alpha = 4$ deg.

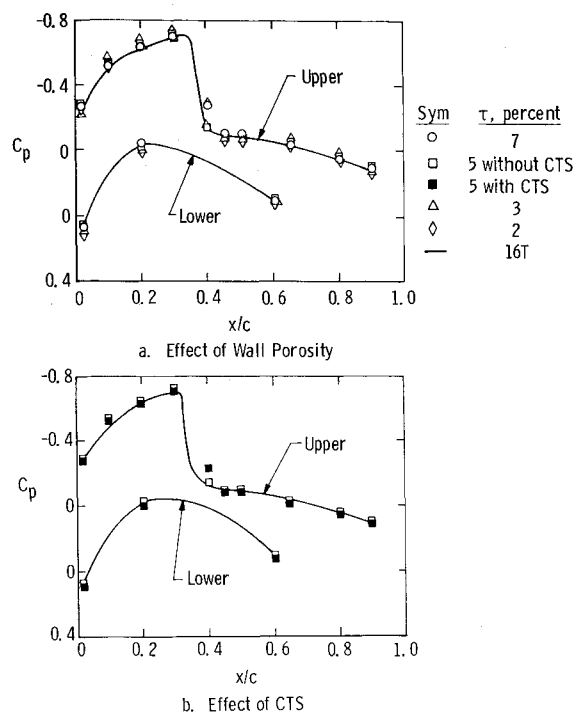

Fig. 9 Interfering inputs at tail location, $M_\infty = 0.9$ and $\alpha = 4$ deg.

slightly supercritical and the flow at the control surface is very subcritical. In fact, the disturbance at the control surface for $M_\infty = 0.7$, $\alpha = 4$ deg was of similar magnitude as the measurement accuracy. Of particular interest are the cases for Mach numbers 0.9 and 0.95. The flow over the model lifting surfaces at $M_\infty = 0.9$ is predominantly supercritical; however, the flow at the control surface remains subcritical. Both the flow over the model lifting surfaces and at the control surface contain supercritical regions at $M_\infty = 0.95$.

Mach Number 0.9

The pressure distribution at the control surface location is shown for several lateral tunnel stations in Fig. 7a for the standard tunnel wall configuration of 5% porosity on all four walls. Included are the measured tunnel data along with the calculated distribution corresponding to unconfined flow for the measured normal velocity distribution. The upper surface distribution indicates the pressure in the region of the peak

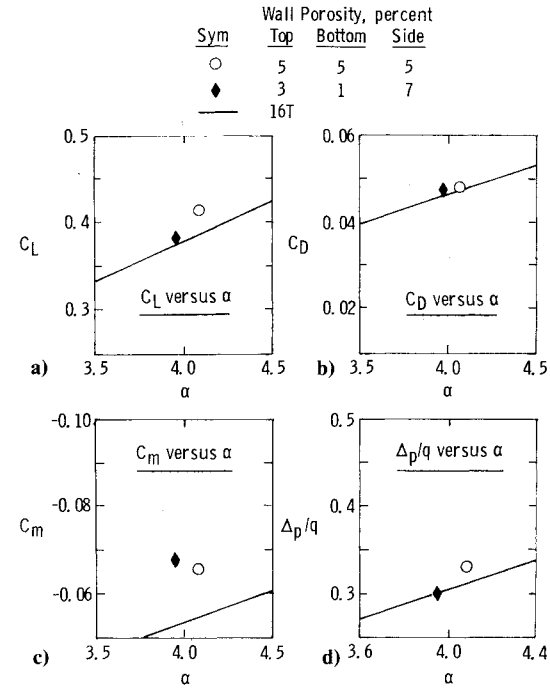

Fig. 10 Model force and nose differential pressure coefficients, $M_\infty = 0.9$ and $\alpha = 4$ deg.

should be decreased while the lower surface distribution has a different longitudinal trend from that required.

As discussed previously, the procedure was to adjust the top wall first. Therefore, the top wall porosity was reduced to lower the peak pressure. The result for 3% porosity on the top wall is shown in Fig. 7b. The bottom wall was then adjusted keeping the top wall fixed at 3% porosity and the side walls fixed at 5% porosity. The best agreement of the pressure distribution on the lower control surface, when compared with that required, was with a bottom wall porosity of 1%. Note that either top or bottom wall adjustments had negligible effect on the opposing control surface distribution as seen in Figs. 7a-7c. Further improvement at the lower control surface was finally obtained by adjusting the side wall porosities to 7%, with the resulting control surface pressure distribution shown in Fig. 7d.

At this point in the experiment, iterations on these test conditions were stopped. The comparisons shown in Fig. 7d could probably be improved somewhat by further fine tuning of the individual wall porosities; however, these results were deemed sufficient for demonstration purposes. It is very interesting to note that the average porosity of the four walls is 4.5% which is approximately that given by classical wall interference theory to be required for minimum blockage interference[8] at $M_\infty = 0.9$.

The pressure distribution on the model wing and tail surfaces is shown in Fig. 8. Comparing the model data with the wall interference-free results from Tunnel 16T demonstrates consistency with the control surface information (Fig. 7), with the exception of the tail upper surface. Although the data from Tunnels 16T and 4T were obtained at the same P_T and chord Reynolds number, there is still evidence of Reynolds number effects on the aft portion of the wing distribution, predominantly for the 90% span location. Otherwise, the agreement for the final adjusted wall configuration is very good.

Two possible causes for the disagreement of the tail upper surface pressure distribution from the Tunnel 16T data are a lack of longitudinal wall control variation or interference from the proximity of the CTS to the model tail. The model tail pressure distribution for a uniform variation of wall porosity on all walls is shown in Fig. 9a. These data were

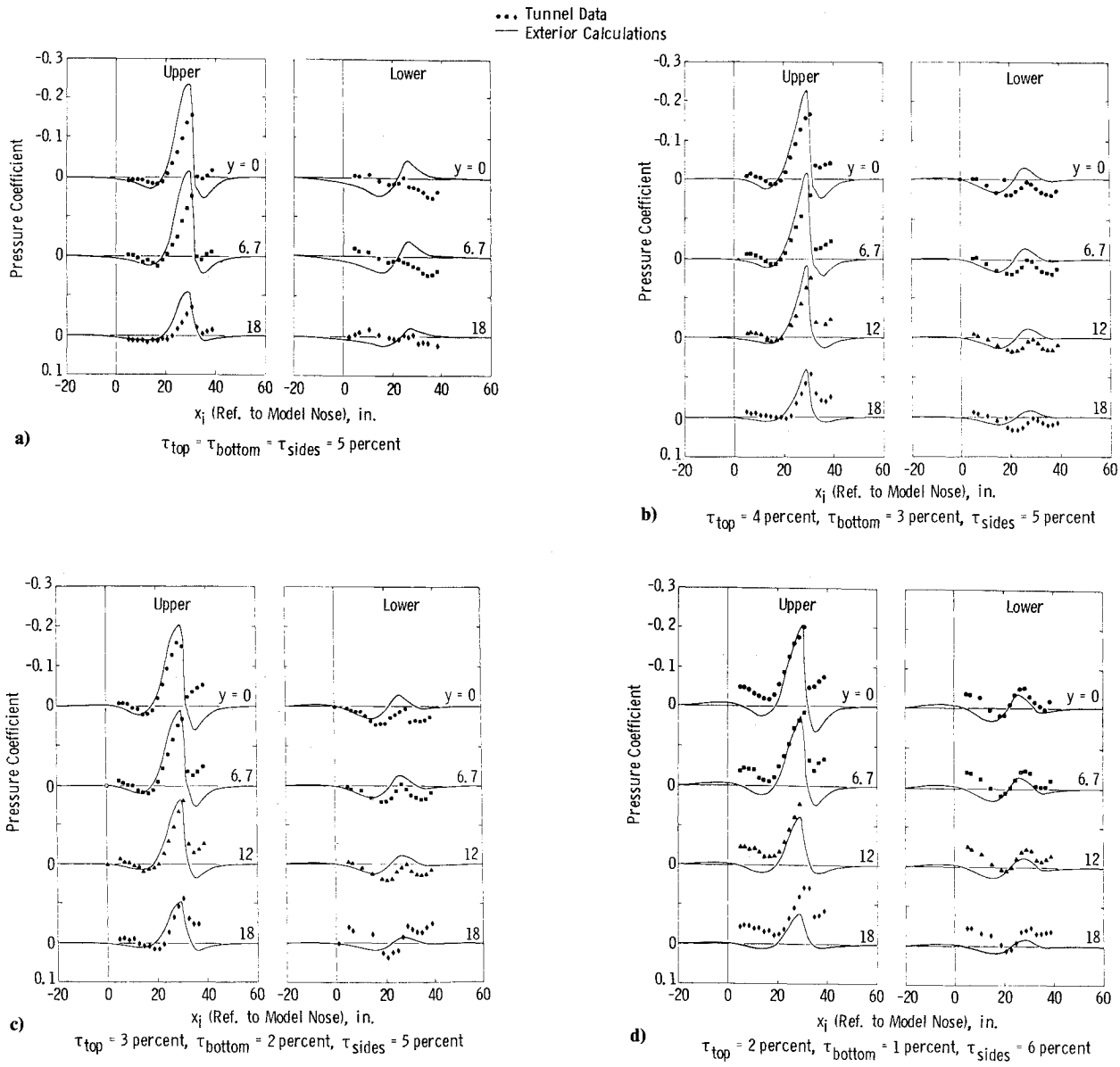

Fig. 11 Control surface presure distribution, $M_\infty = 0.95$ and $\alpha = 4$ deg.

obtained without the CTS installed. The trend with porosity reverses at approximately 5% porosity where the best agreement also occurs. The distribution for 3% porosity (the value of the top wall for the final adjusted case) is still in good agreement with the Tunnel 16T data. The pressure distribution on the tail at 5% uniform porosity with and without the CTS installed is shown in Fig. 9b. The presence of the CTS has a definite influence on the model tail. It is felt, however, that the available information is inconclusive as to the cause of the tail data divergence.

A comparison of the model force data is shown in Figs. 10a-10c. Significant improvement was demonstrated for the lift coefficient. The drag coefficient was essentially unchanged, and no improvement was experienced for the pitching moment coefficient as a result of the effects on the tail as shown in Fig. 8. The model nose design was similar to a hemispherical head flow angle sensor. The nose pressure differential in the pitch plane is shown in Fig. 10d. The data indicate that the incidence of the model nose relative to the stream was in agreement with that for the interference-free data. With globally variable porosity walls, an advantage of the adaptive technique is that it can compensate for planar tunnel flow angularity.

Mach Number 0.95

The control surface pressure distribution for Mach number 0.95 and a 4 deg angle of attack is shown in Fig. 11. Note that at these conditions the distribution at the control surface is supercritical. The distribution for the standard tunnel configuration of 5% uniform porosity on all walls is shown in Fig. 11a. Again, the exterior calculations indicate the upper surface pressure about the peak should be decreased and the lower surface has a different longitudinal trend from that required. The walls were adjusted and two of the intermediate iterations are shown in Figs. 11b and 11c. The iterations were stopped with the configuration indicated in Fig. 11d. Again, the results are not intended to represent the best results obtainable but were taken as a convenient concluding point.

The $M_\infty = 0.95$ data indicate a requirement for lateral porosity variation as shown in the comparisons of the measured and computed pressure distributions at various lateral locations (Fig. 11). The criterion selected to adjust the walls in the present experiment was the distribution at the centerline ($y = 0$) where the magnitude of the model disturbance field is a maximum. The variations with lateral location may be misleading and actually irritated by an error in the calculated distribution. It was discovered early in the conduct

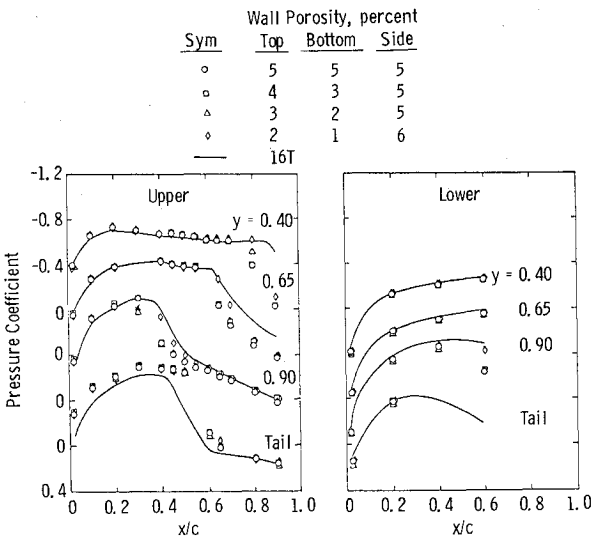

Fig. 12 Model wing and tail pressure distribution, $M_\infty = 0.95$ and $\alpha = 4$ deg.

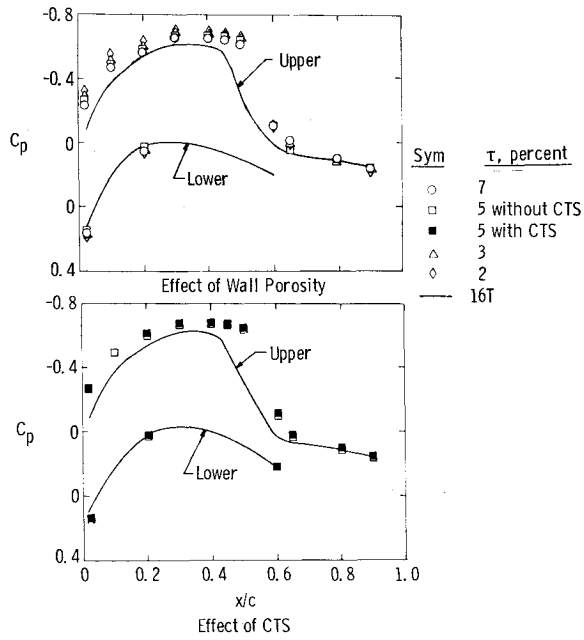

Fig. 13 Interfering inputs at tail location, $M_\infty = 0.95$ and $\alpha = 4$ deg.

of the experiment that large errors were introduced in the external computational results by insufficient specification of the side control surface flow angle distribution. The flow velocity normal to the side wall reverses sign from above to below the model wing with large gradients in the vicinity of the wing. A sufficient number of measurements to define the surface could not be made in the area where these gradients occur because of the CTS limitations. It was found that minimal error was introduced at the upper and lower surface by specifying the lateral surface normal velocity to be zero. Analytical simulations are planned to clarify this presumption. The model wing and tail surface pressure distribution is shown in Fig. 12. Significant improvement is demonstrated on the wing surface pressure distribution. There is no degradation in the wing pressure data toward the outboard span location. In fact, the reverse is shown, indicating that the lateral variation at the control surface has negligible effect at the model location or is indeed a computational error attributable to the sidewall boundary conditions.

The wall adjustments were ineffectual on the tail pressure distribution. The effect of uniform porosity variation without the CTS installed and the effect of the CTS on the tail are

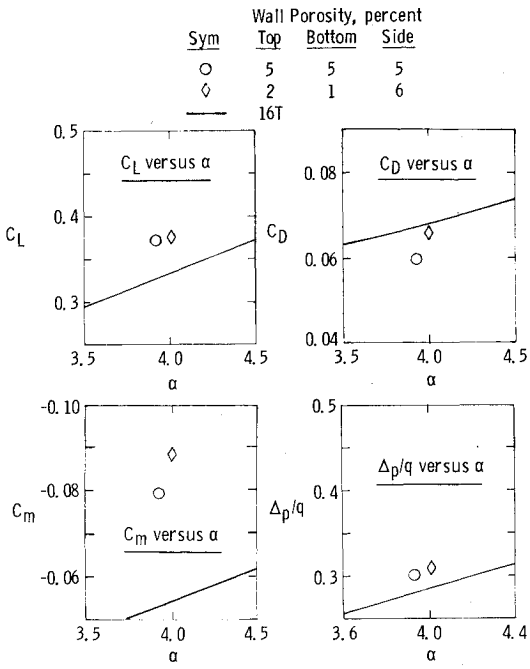

Fig. 14 Model force and nose differential pressure coefficients, $M_\infty = 0.95$ and $\alpha = 4$ deg.

shown in Fig. 13. The tail pressure distribution was insensitive to either effect.

Comparison of the model force data is shown in Fig. 14. No significant improvement of the force data was demonstrated at $M_\infty = 0.95$.

Conclusions and Recommendations

Preliminary experiments were conducted in Tunnel 4T employing the adaptive wall technique to adjust the individual wall porosities to reduce the wall interference on a three-dimensional, transonic model configuration. The objective was to evaluate the effectiveness of global porosity variation for three-dimensional flows and to identify areas of concern for future adaptive wall development.

Wall adjustments based on the control surface measurements and exterior region calculations resulted in improvement on the wing surface pressure distribution at each of the conditions. General improvement of the force data was experienced at $M_\infty = 0.7$ and 0.9. Agreement of the pressure distribution with interference-free data was not obtained at the tail location for $M_\infty = 0.9$ and 0.95 and consequently the pitching moment was in error when compared to the interference-free values. The CTS was shown to have a significant effect on the model tail; however, the available information was not sufficiently conclusive to identify the tail phenomenon as CTS interference or a deficiency of the global wall control in the presence of a strong longitudinal gradient.

Additional experiments are recommended using a control surface variable measurement technique that does not interfere aerodynamically or physically with the test model. Also, the control surface variable measurement system should have expanded longitudinal motion capabilities. Iterations are required at additional test conditions, including reasonable ranges of angle of attack at given sets of tunnel conditions, to identify the capabilities of the variable porosity walls more clearly.

Acknowledgments

The research reported herein was performed by the Arnold Engineering Development Center (AEDC), Air Force Systems Command. Work and analysis for this research were done by personnel of AEDC. Further reproduction is authorized to satisfy needs of the U.S. Government.

References

[1] Kraft, E.M. and Parker, R.L., Jr., "Some Experiments with the Reduction of Boundary Interference by Adaptive Wall Technology," AEDC-TR-79-51, 1979.

[2] Ferri, A. and Baronti, P., "A Method for Transonic Wind-Tunnel Corrections," *AIAA Journal,* Vol. 11, Jan. 1973, pp. 63-66.

[3] Sears, W.R., "Self-Correcting Wind Tunnels," Calspan Rept. RK-5070-A-2, July 1973; also *Aeronautical Journal,* Vol. 78, Feb./March 1975, pp. 80-89.

[4] Lo, C.F. and Kraft, E.M., "Convergence of the Adaptive-Wall Wind Tunnel," *AIAA Journal,* Vol. 16, Jan. 1978, pp. 67-72.

[5] Murman, E.M., Bailey, F. R., and Johnson, M.L., "TSFOIL—A Computer Code for Two-Dimensional Transonic Calculations, Including Wind-Tunnel Wall Effects and Wave-Drag Evaluation," NASA SP-347, March 1975, pp. 769-788.

[6] Bailey, F.R. and Ballhaus, W.F., "Comparisons of Computed and Experimental Pressures for Transonic Flows about Isolated Wings and Wing-Fuselage Configurations," NASA SP-347, March 1975, pp. 1213-1231.

[7] "Propulsion Wind Tunnel Facility," *Test Facilities Handbook* (11th ed.), Vol. 4, Arnold Engineering Development Center, June 1979.

[8] Lo, C.F. and Oliver, R.H., "Boundary Interference in a Rectangular Wind Tunnel with Perforated Walls," AEDC-TR-70-67 (AD704123), April 1970.